

DETECTION AND CHARACTERISATION OF ATMOSPHERIC AEROSOL USING SIMULATED MEASUREMENTS FROM ENVISAT-1 NADIR VIEWING SPECTROMETERS

F. Torricella¹, E. Cattani¹, M. Cervino¹, M. J. Costa^{1,2} and V. Levizzani^{1*}

¹Institute of Atmospheric and Oceanic Sciences, ISAO-CNR, via Gobetti 101, I-40129 Bologna, Italy

²University of Évora, Dept. of Physics, R. Romão Ramalho 59, P-7000 Évora, Portugal

ABSTRACT

The load of tropospheric aerosol from natural and anthropogenic sources is of crucial importance for the determination of the Earth radiative balance and the prediction of climate changes. The nadir-viewing spectrometers (AATSR, MERIS, and SCIAMACHY) onboard the ENVISAT-1 platform, to be launched mid 2001, will be independently operated and are conceived for different atmospheric studies. The spatial overlap of their swaths and time coincidence of their measurements, however, make them all part of an ideal hyper-instrument with enlarged spectral coverage from the UV (covered at high spectral resolution by SCIAMACHY) to the IR of the AATSR channels. The use of thermal channels greatly helps in discriminating cloud-contaminated scenarios prior to aerosol retrieval. A sensitivity test is presented for assessing the performances of such an *hyper-instrument* in the retrieval of aerosol optical thickness and characterisation of aerosol type. The test is performed considering a generic retrieval method in which satellite radiances are interpreted by best fitting the measurements to calculated spectra for one or more standard aerosol models. A large set of radiance spectra computed by varying the main parameters affecting the atmospheric response and the aerosol loading is analysed. The spectral characteristics and the different spatial scales of the various instruments are properly taken into account.

1. INTRODUCTION

Satellite-based instruments conceived for the study of the atmosphere's scattering constituents, specifically aerosol and clouds, are designed to include more spectral channels and have a higher spectral and spatial resolution than other instruments aimed to ocean colour, sea surface temperature, atmospheric chemistry or land cover. Note that the large spectral span from the UV to the IR, which is required to successfully detect and characterise these variable atmospheric

* *Visiting Scientist at EUMETSAT, Darmstadt, Germany*

components, is very demanding for a single instrument. Each spectral range requires in fact different sensors, observation techniques, and spectral resolution. A proper cloud clearing is a mandatory *a priori* requirement to perform an accurate aerosol retrieval, so that the use of IR measurements simultaneous to those in the UV-VIS is crucial. The ENVISAT-1 mission, planned to be launched in June 2001, carries, among other sensors, the nadir-viewing SCanning Imaging Absorption spectroMeter for Atmospheric CHartographY (SCIAMACHY), the MEdium Resolution Imaging Spectrometer (MERIS) and the Advanced Along Track Scanning Radiometer (AATSR). They are all nadir looking instruments, or including a nadir-viewing mode. Simultaneous, high quality and calibrated measurements of the same ground target from the ultraviolet (UV) to the infrared (IR) will be available (Fig. 1). These instruments, although independently operated and aimed to different atmospheric studies, can be regarded in principle as a single *hyper-instrument* with enlarged spectral coverage, due to the spatial overlap of their swaths and the time coincidence of the measurements. A sensitivity analysis is presented that assesses the performances of a generic fitting method (the one of Torricella *et al.*, 1999) in retrieving the aerosol characteristics when combining the MERIS channels, the UV measurements of SCIAMACHY and the near infrared (NIR) to infrared measurements of AATSR. The analysis focuses on complex scenarios with aerosol loading, partial cloud coverage and varying aerosol type (this latter is simulated by varying the aerosol humidity level, see section 3). This kind of scenario is an ideal testbed for satellite-based retrieval methods. Large aerosol transport events and small cloud contamination induce very similar radiative responses over the visible (VIS) to NIR wavelength range, but impact very differently on radiative forcing and climate in general. Note that only multi-angle observations (for example from the MISR instrument flying on the TERRA mission) of the same target will allow to discriminate among the various aerosol mixtures and thin clouds (e.g. cirrus) from high aerosol loadings with a high confidence degree. Nevertheless classical, well established, simple methods based on spectral radiance fitting still deserve attention for some applications, especially with the inclusion of more NIR and IR channels.

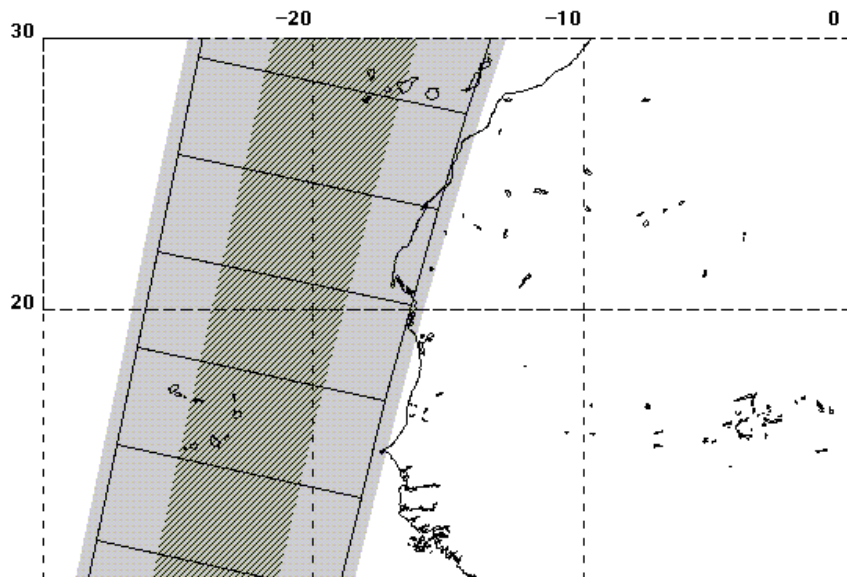


Figure 1. Example of superimposition of AATSR, MERIS and SCIAMACHY swaths for one ENVISAT-1 descending orbit overpassing the Cape Verde islands. Solid box: MERIS. Hollow box: SCIAMACHY. Dashed box: AATSR.

2. INSTRUMENTS AND MEASUREMENTS

MERIS, SCIAMACHY and AATSR are spectrometers/spectroradiometers that measure the radiation reflected/emitted by the atmosphere-surface system in the UV-VIS-NIR-IR part of the electromagnetic spectrum. Each one has its own capabilities for the detection and characterisation of clouds and aerosol field. AATSR (Murray *et al.*, 1999) is a dual-view, self-calibrating, VIS and IR radiometer. It carries out measurements of TOA reflectance/brightness temperature for land surface, atmosphere, clouds, and ocean studies. AATSR observes the same scene along the direction of the orbit track first at an incident angle of 55 deg (forward scan) and then (150 s later) at an angle close to the nadir. The curved swaths are 500 km long with the one at nadir consisting of 555 pixels, $1 \times 1 \text{ km}^2$ at the centre. MERIS (Rast *et al.*, 1999) is an along-track, push-broom imaging spectrometer conceived primarily for oceanographic and secondarily for atmospheric and land observations. MERIS works with up to 16 spectral bands, whose width and position are programmable in-flight in the 0.390 to 1.040 μm spectral range, and a spectral resolution of 2.5 nm. MERIS data are characterised by two spatial resolutions: full resolution (FR) with a pixel size of $300 \times 300 \text{ m}^2$ at nadir, and a reduced resolution (RR), achieved by a combination of 4×4 adjacent pixels across-track and along-track, resulting in a $1200 \times 1200 \text{ m}^2$ resolution at nadir. SCIAMACHY (Bovesmann *et al.*, 1999) is a moderate resolution imaging spectrometer, conceived for studies of the chemistry and physics of the Earth's atmosphere. SCIAMACHY has three measurement modes, nadir, limb and solar/lunar occultation, but in this work only the nadir mode is considered. In this mode each full scan covers an area of approximately 30 km along-track and 960 km across-track, with a typical spatial resolution of $30 \times 240 \text{ km}^2$. The spatial resolution can be increased up to $30 \times 60 \text{ km}^2$ in selected spectral windows (e.g. UV) to investigate key atmospheric constituents, such as clouds and aerosols, at their appropriate spatial scales. As a working hypothesis the instruments are considered to look at the nadir with the same observing geometry and at the very same time. Slight differences in the observing conditions are accounted for when considering the overall error associated with the method.

3. THE SIMULATED SPECTRA

The radiative transfer model MODTRAN (Berk *et al.*, 1998) was selected for the simulations of the ENVISAT spectra. The model computes the intensity of the radiation reflected/emitted by the atmosphere accounting for all the main physical processes, and including the standard vertical profiles of the atmospheric components of paramount importance. The inputs used in the simulations are summarized in Table 1. Aerosol spectral optical properties over the whole range 0.3-12.5 μm were derived from the aerosol database of Levoni *et al.* (1997) and were input to MODTRAN as user-supplied parameters. The URBAN aerosol class at 7 humidity levels (relative humidity, $RH = [0, 99] \%$) was selected. The choice yields to a transition from a moderately absorbing type (dry) to a non-absorbing type (humid), the latter being associated to almost spectrally-independent extinction properties. Moreover, an increase in RH reflects in an increase of the size of the aerosol particles, thereby altering the size distribution. This fact should increase the relevance of the NIR channels in the aerosol type recognition. This approach allows to cover a number of different aerosol regimes, depending on RH and the aerosol optical thickness at 0.550 μm

(τ_A) without the need of fixing, for instance, the complex refractive index of aerosol. In fact the increasing RH level reverberates on both refractive index and size distribution according to Hänel's theory (Levoni *et al.*, 1997). The aerosol was confined to the 0-2 km atmospheric layer and τ_A was varied as in Table 1 so as to represent aerosol loadings from almost clear to very turbid atmospheres. The observation geometries are those of the typical nadir-viewing sensors. Two kinds of surface spectral lambertian albedoes were adopted, the dark sea surface and the strong reflecting sand, to emphasize the different behavior of absorbing and non-absorbing particulate above nonreflecting or strongly reflecting surfaces. The boundary temperature was set to 30°C for the sand and 15°C for the sea. The aerosol-loaded spectra were linearly combined with cloudy spectra to simulate scenarios with different cloud coverage (f , see Table 1). The cloudy spectra were obtained by selecting stratus/stratocumulus clouds with a optical thickness of 50 in the VIS and top height of 8 km. The corresponding spectral radiances obtained from MODTRAN are regarded as high resolution spectra, i.e. they simulate the spectral radiance incident upon the instruments' entrance slit. A software was developed to compute the radiance output of the three instruments by convolving the high resolution spectra with the suitable slit functions of the various channels. Table 2 reports the list of the channels of the three instruments that compose the spectral coverage of the hyper-instrument. The SCIAMACHY channels affected by gas absorption features were not considered. The resolution was degraded to 1.0 nm for smoothing solar spectral features. The nine channels with variable resolution cover a spectral range from 0.364 to 3.7 μm . The two thermal IR AATSR channels at 11 and 12 μm have been separately processed (see next section). Note that the SCIAMACHY spatial resolution is much more coarse than those of MERIS and AATSR, so that the use of UV wavelengths implies that MERIS and AATSR measurements had to be degraded to SCIAMACHY resolution. This is a relevant issue and will be commented later on. At this stage the problem is avoided by carrying out the analysis as if the scenarios were uniform at the worst spatial scale

4. ANALYSIS TOOLS

After computing the radiances measured by the hyper-instrument for the scenarios described in the previous section, the distinguishability of the spectra was analyzed. We designate a spectrum at time a time as “measurements”. We then test whether the “measured” radiances can be distinguished, within the instrument uncertainty plus model errors, against “comparison” spectra. This is accomplished by computing the χ^2 distance between the measured spectrum $R_M(\lambda_i, SURF; \theta_0, \tau_A^*, RH^*, f^*)$ and all the remaining spectra $R_C(\lambda_i, SURF; \theta_0, \tau_A^j, RH^k, f^l)$ according to:

$$\chi_{j,k,l}^2 = \frac{1}{N_{wl}} \sum_{i=1}^{N_{wl}} \frac{(R_M(\lambda_i, SURF; \vartheta_0; \tau_A^*, RH^*, f^*) - R_C(\lambda_i, SURF; \vartheta_0; \tau_A^j, RH^k, f^l))^2}{R_M(\lambda_i, SURF; \theta_0; \tau_A^*, RH^*, f^*)^2}$$

$$N_{wl} = 9 \quad j = 1, \dots, 9 \quad k = 1, \dots, 7 \quad l = 1, \dots, 14$$

where the symbols are defined in Table 1.

The χ^2 is analogously and separately computed for the two AATSR IR wavelengths. The separation was necessary because previous analyses revealed that including these two wavelengths among the UV-VIS-NIR greatly decreases their usefulness in detecting the cloud coverage, due to the smaller overall variability of atmospheric radiances in the IR with respect to the UV-VIS. Moreover, the

assessment of the aerosol effects in the IR requires a deep knowledge of the spectral emissivity (depending also upon particle size) and thus these two channels were used only to evaluate the sensitivity to cloud coverage. The χ^2 is not divided by the error value σ^2 because σ^2 is assumed to be the same for each channel. The analysis of the shape of the χ^2 function, depending on f , τ_A and the surface type (sea or sand), provides an idea of the robustness of a generic pseudo-inversion method based on the fitting of measurements to the computed spectra. The ideal condition is that the χ^2 function has a single minimum and the shape of the function near the minimum is steep enough for the retrieval of the aerosol parameters with acceptable uncertainty. The χ^2 hyper-surface is represented as contour plots on planes that intersect it at a fixed value of one of the parameters. The minimum of the χ^2 function determines the retrieved parameters relative to the pseudo-measured scenario. In any real condition the absolute minimum value of χ^2 will not be zero due to various error sources (model and measurement errors). The most appropriate way of examining this kind of plots is by selection of a contour level as representative of the overall error inherent to the method and/or measurements (we adopt the 10% threshold, corresponding to $\chi^2=0.01$). All the triplets (f , τ_A , RH) falling inside this isopleth cannot be distinguished at an error level of 10%. Contour levels encompassing small areas well centered around the true value imply that the retrieval has good chances of retrieving precise and accurate parameters.

5. DISCUSSION AND CONCLUSIONS

The results for some relevant cases are presented as contour plots of χ^2 depending on the parameters (f , τ_A , RH) (Fig. 2). In Fig. 2 the χ^2 values are displayed in the 3-D space with RH in abscissa (covering the range [0, 99] %), τ_A on the y axis ([0.01, 3]), and the cloud fraction f on the z axis covering different ranges in panels (A), (B), (C) and (D). In each case we wanted to show only the planes $f=f^l$ having χ^2 values less than 10^{-2} (see the red areas and at the innermost darker regions). All planes not shown either do not display red areas or were not included in the analysis (having $f > 30\%$).

The following conclusions could be drawn from the analysis of all the simulated cases. Small cloud fractions ($f^* \leq 10\%$ over the sea and $f^* \leq 5\%$ over the sand) are retrieved from IR data only if dry aerosol is present over the scenario, both over the sea and sand. For humid aerosols there is a complete trade off between humidity and cloud fraction, especially for high values of τ_A (Fig. 2 (A)). Spectra characterized by low cloud fractions and high values of RH are not distinguishable from the pseudo-measured spectrum as well as from spectra characterized by high cloud fractions and low RH values. This can be seen in (A) by noting that χ^2 minima (red and darker areas) are moving in the (τ_A , RH) planes depending on the value of f : increasing f induces the minimum to shift towards lower (wrong) values of RH . For higher values of f^* the retrieval is more accurate, because even the highest value of RH cannot match high values of f^* . For instance $f^*=30\%$ (Fig. 2 (B)) leads to retrieved $f > 25\%$ (no upper limit is given because our analysis is restricted to $f \leq 30\%$). Pay attention to the z scale, starting at 25%) with the actual value depending on τ_A^* . The only relevant exception are the scenarios with dry aerosol over the sand, for which the cloud fraction retrieval remain problematic also for $f^*=30\%$. For low values of the optical thickness the cloud fraction is in general well retrieved, except for high cloud coverage over the sand. Our results suggest that in the IR even low aerosol loadings ($\tau_A^*=0.2$) can be mismatched with partial cloud coverage ($f < 30\%$), especially if the aerosol is highly humidified. Cloud fractions as low as 5% are

found to destroy the aerosol information content of such large spectral interval if the aerosol loading is small ($\tau_A^* < 0.5$) at the selected accuracy level. Assuming an overall accuracy of 3% (corresponding to the 10^{-3} isopleth) will, however, allow the retrieval of aerosol characteristics also at $f^* = 30\%$. For clear scenarios we found that the hyper-instrument is able of retrieving small τ_A^* over the sand only if $RH = 0\%$ while high aerosol loadings ($\tau_A^* > 1$) are retrieved over both sand and sea, with smaller errors over the sand if the aerosol is dry and over the sea if the aerosol is humid (see Fig. 2 (C) and (D)). For instance $\tau_A^* = 3$ is retrieved over the sand as > 2.7 if dry and > 0.9 if humid and, over the sea as > 2 if dry and > 2.8 if humid. The relative humidity is undetermined for small τ_A^* but is very well retrieved ($\Delta RH < 10\%$) for $\tau_A^* > 1$.

The results are representative examples of the large set of graphs we produced, showing different behaviours over sea and sand. The representation of such multi-variate results is a challenging task, and it is perhaps the weakest aspect of this kind of sensitivity analysis. We are still analysing the results trying to achieve a more quantitative assessment of the performance of the method.

As mentioned before the different spatial resolutions of the three instruments, introduce some ambiguity in the definition of the quantities τ_A^* , RH^* and f^* for non-homogeneous scenarios. Nevertheless, the conclusions drawn from the present analysis are applicable to any spectrometer covering such a large spectral interval. In the specific case of ENVISAT-1 instruments the better approach for the analysis of non-uniform scenarios will probably be of separately processing SCIAMACHY data (i.e. the data at the coarser spatial scale) in order to derive some information on aerosol type prior to process MERIS and AATSR data. For instance the UV SCIAMACHY measurements allow to derive a TOMS-like Aerosol Index (Torres *et al.*, 1998) useful to discriminate the presence of absorbing aerosol over the scenario.

Variable	Symbol	Number of values	Selected value(s)
Observer zenith angle	θ	1	0 deg
Sun zenith angle	θ_0	2	15, 45 deg
Spectral ground albedo	$A_g(\lambda)$	2	Ocean, Sand
Relative humidity (%)	RH	7	0, 70, 80, 90, 95, 98, 99
Aerosol optical thickness at 550 nm	τ_A	9	0, 0.01, 0.05, 0.1, 0.2, 0.5, 1, 2, 3
Cloud fraction (%)	f	4	0, 5, 10, 20, 30

Table 1. Input values for creating the set of simulated spectra.

SCIAMACHY	0.364 (1.0)	0.373 (1.0)	0.394 (1.0)	0.424 (1.0)
MERIS	0.753 (7.5)	0.775 (12.5)	0.890 (10.0)	
AATSR	1.6 (300.0)	3.7 (300.0)		

Table 2. Central wavelengths (μm) of the selected channels from the three instruments. In brackets the bandwidths (nm).

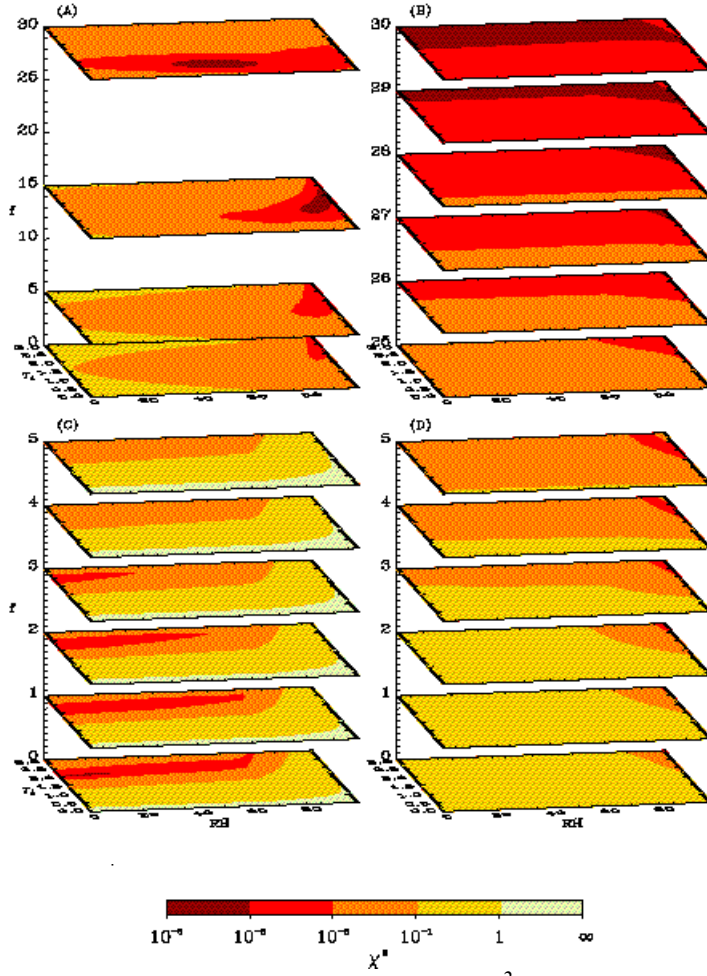


Figure 2: Examples of contour plots of the χ^2 function depending on (f, τ_A, RH) . (A) is for a pseudo-measured scenario characterised by $\theta_0=15^\circ$, sand, $\tau_A^*=3$, $RH^*=99\%$, $f^*=5\%$. (B): $\theta_0=15^\circ$, sea, $\tau_A^*=3$, $RH^*=0\%$, $f^*=30\%$. (C): $\theta_0=15^\circ$, sand, $\tau_A^*=2$, $RH^*=99\%$, $f^*=0\%$. (D): $\theta_0=15^\circ$, sea, $\tau_A^*=3$, $RH^*=99\%$, $f^*=0\%$. (A) and (B) are derived from IR measurements only (see text). (C) and (D) are computed using the hyper-instrument wavelengths.

ACKNOWLEDGEMENTS

We would like to thank Pierre Viau from ESA-ESTEC for supplying the CFI-ESOV software needed to display ENVISAT-1 instruments' swaths.

REFERENCES

- Berk, A., L. S. Bernstein, G. P. Anderson, P. K. Acharya, D. C. Robertson, J. H. Chetwynd, and S. M. Adler-Golden, 1998: MODTRAN cloud and multiple scattering upgrades with application to AVIRIS. *Remote Sens. Environ.*, **65**, 367-375.
- Bovesmann, H., J. P. Burrows, M. Buchwitz, J. Frerick, S. Noel, V. V. Rozanov, K. V. Chance, and A. P. H. Goede, 1999: SCIAMACHY: Mission objectives and measurement modes. *J. Atmos. Sci.*, **56**, 127-150.
- Levoni, C., M. Cervino, R. Guzzi, and F. Torricella, 1997: Atmospheric aerosol optical properties: A database of radiative characteristics for different components and classes. *Appl. Opt.*, **36**, 8031-8041.
- Murray, J., P. Bailey, A. Birks, and D. Smith, 1999: ATSR-1/2 user guide, edited by C. Mutlow. 29 pp., <http://www.atsr.rl.ac.uk/>.
- Rast, M., J. L. Bézy, and S. Bruzzi, 1999: The ESA Medium Resolution Imaging Spectrometer MERIS - A review of the instrument and its mission. *Int. J. Remote Sensing*, **20**, 1681-1702.
- Torres, O., P. K. Barthia, J. R. Herman, Z. Ahmad, and J. Gleason, 1998: Derivation of aerosol properties from satellite measurements of backscattered ultraviolet radiation: Theoretical basis. *J. Geophys. Res.*, **103**, 17099-17110.
- Torricella, F., E. Cattani, M. Cervino, R. Guzzi, and C. Levoni, 1999: Retrieval of aerosol properties over the ocean using Global Ozone Monitoring Experiment measurements: Method and application to test cases. *J. Geophys. Res.*, **104**, 12085-12098.